Polyimide−Silica Composite Materials: How Does Silica Influence Their Microstructure and Gas Permeation Properties?

C. Joly,[†,||] M. Smaihi,*[,†] L. Porcar,[‡] and R. D. Noble[§]

LMPM, UMR 5635, CNRS-ENSCM-UM2, 8 rue de l'Ecole Normale, 34296 Montpellier, Cedex 5, France, Groupe de Dynamique des Phases Condensées, UMR 5581, CNRS-UM2-CC026, Place Eugène Bataillon, 34095 Montpellier Cedex 5, France, and University of Colorado at Boulder, CB 424, Boulder, Colorado 80309-0424

Received July 15, 1998. Revised Manuscript Received June 18, 1999

Composite polyimide−silica materials have been synthesized via the sol−gel process and their gas transport properties studied. Structural characterizations have been performed showing that materials prepared with large concentration of silicon alkoxyde are composites made of silica particles embedded in the polyimide matrix while low-silicon alkoxyde concentration induces homogeneous materials. X-ray diffraction shows that the presence of silicon species induces modifications in the microstructure of the polyimide chains. These modifications have been confirmed by a shift of the glass transition temperature and density variations. Influence of the temperature and silicon species on the gas transport have been studied using various gases (nitrogen, oxygen, carbon dioxide, and methane) showing that gas permeation coefficients increase with the silicon species proportion. CO_2 sorption measurements have been performed at various temperatures and the results have been analyzed in terms of the dual sorption theory. Activation energies have been calculated for the permeation and sorption mechanisms. These results show that silicon species contributes to the overall permeability.

Introduction

Hybrid organic−inorganic materials[1] have become an expanding field of research as the introduction of organic molecules can improve the characteristics of a matrix. They are generally obtained via a sol−gel process. Among these materials, polyimide−silica materials have become increasingly studied.[2−16]

In polyimide−silica composites prepared via a sol−gel process, silica particles are dispersed in a polyimide matrix.[2−9,15−16] Polyimide−silica hybrids have been prepared using precursors which can provide chemical bonding between the organic and the inorganic phase.[10−14]

A previous study[15] showed that the microstructure of polyimide−silica composite materials can be tailored by adjusting the silica proportion and the hydrolysis ratio parameters. The increase of the silica proportion induces an increase of the silica particle size. An increase of the hydrolysis ratio has the same consequences.

Gas transport properties of these materials have been studied by comparing a pure polyimide film with a sample containing 35 wt % silica.[16] The results showed that the presence of silica drastically modifies the gas permeation properties.

The present study broadens these data by varying the silica proportion and temperature. The structural characteristics of these samples have been studied by scanning electron microscopy (SEM), density measurements, thermogravimetric analysis (TGA), dynamic mechanical thermal analysis (DMTA), X-ray diffraction,

* Corresponding author: smaihi@crit1.univ-montp2.fr.
† LMPM, UMR 5635, CNRS-ENSCM-UM2.
‡ Groupe de Dynamique des Phases Condensées, UMR 5581, CNRS-UM2-CC026.
§ University of Colorado at Boulder.
|| Present address: Laboratoire de Pharmacognosie, UPRESA 6013, Moulin de la Housse, CPCB Bat. 18, BP 1039, 51097 REIMS Cedex 2.

(1) (a) Sanchez, C.; Ribot, F. *New J. Chem.* **1994**, *18*, 1007. (b) Novak, B. M. *Adv. Mater.* **1993**, *5*, 422.
(2) (a) Morikawa, A.; Iyoku, Y.; Kakimoto, M.; Imai, Y. *Polym. J.* **1992**, *24* (1), 107. (b) Morikawa, A.; Iyoku, Y.; Kakimoto, M.; Imai, Y. *J. Mater. Chem.* **1992**, *2* (7), 679. (c) Morikawa, A.; Yamaguchi, H.; Kakimoto, M.; Imai, Y. *Chem. Mater.* **1994**, *6*, 913.
(3) Iyoku, Y.; Kakimoto M.; Imai, Y. *High Perform. Polym.* **1994**, *6*, 43.
(4) Mascia, L.; Kioul, A. *J. Mater. Sci. Lett.* **1994**, *13*, 641.
(5) Nandi, M.; Conklin, J. A.; Salvati, L., Jr.; Sen, A. *Chem. Mater.* **1991**, *3*, 201.
(6) Moaddeb, M.; Koros, W. J. *J. Membr. Sci.* **1997**, *125* (2), 143.
(7) Hu, Q.; Marand, E.; Dhingra, S.; Fritsch, D.; Wen, J.; Wilkes, G. *J. Membr. Sci.* **1997**, *135* (1), 65.
(8) Spinu, M.; Brennan, A.; Rancourt, J.; Wilkes, G. L.; McGrath, J. E. *MRS Symp. Proc.* **1990**, *175*, 179.
(9) Noell, J. L. W.; Wilkes, G. L.; Mohanty, D. K.; McGrath, J. E. *J. Appl. Polym. Sci.* **1990**, *40*, 1177.
(10) (a) Wang, S.; Ahmad, Z.; Mark, J. E. *Polym. Bull.* **1993**, *31*, 323. (b) Wang, S.; Ahmad Z.; Mark, J. E. *Macromol. Rep.* **1994**, *A31, Supplements 3−4*, 411. (c) Wang, S.; Ahmad, Z.; Mark, J. E. *Chem. Mater.* **1994**, *6*, 943.
(11) Ahmad, Z.; Shuhong, W.; Mark, J. E. *ACS Symp. Ser. 585* **1995**, *Chapter 22*, 291.
(12) Mark, J. E.; Wang, S.; Ahmad, Z. *Macromol. Symp.* **1995**, *98*, 731.
(13) Wen, J.; Mark, J. E. *J. Appl. Polym. Sc.* **1995**, *58*, 1135.
(14) Schrotter, J. C.; Smaihi, M.; Guizard, C. *J. Appl. Polym. Sci.* **1996**, *61*, 2137.
(15) Goizet, S.; Schrotter, J. C.; Smaïhi, M.; Deratani, A. *New J. Chem.* **1997**, *21*, 461.
(16) Joly, C.; Goizet, S.; Schrotter, J. C.; Sanchez, J.; Escoubes, M. *J. Membr. Sci.* **1997**, *130*, 63.

10.1021/cm9805018 CCC: $18.00
Published on Web 09/01/1999

Table 1. Data on the Preparation of the Polyimide−Silica Composite Films: Composition of the Starting Solutions and Silica Content in the Final Materials

sample[a]	amic acid unit (10^3 mol)	TMOS (10^3 mol)	molar fraction of TMOS (mol)	silica content (wt %) theor[b]	silica content (wt %) exp[c]
25	1.96	0.67	0.25	5	0
60	1.96	3.09	0.60	20	14
72	1.96	5.04	0.72	30	30
83	1.96	9.87	0.83	45	40

[a] The figure of sample numbers refers to TMOS molar fraction × 100. [b] The theoretical silica content indicates values calculated on the assumption that the sol−gel reactions proceed completely. [c] The experimental silica content indicates the final wt % residue obtained after 750 °C heat treatment in air.

and small-angle X-ray scattering (SAXS) experiments. These results have been combined with gas permeation measurements to point out the role of the silicon species on the modification of the microstructure and the gas permeability of the composite.

Various gases have been used: helium, nitrogen, oxygen, carbon dioxide, and methane. We also studied the influence of temperature on the gas transport properties of these samples. Sorption measurements have been performed at various temperatures and have been analyzed in terms of the dual sorption theory. Activation energies for permeation and sorption mechanisms were calculated.

Experimental Section

1. Material Preparation. The sample preparation has been described in detail elsewhere;[15] it will only be summarized below.

Reference pure polyimide films with poly(4,4-oxydiphenylene pyromellitimide) structure were prepared from 1,2,4,5-benzenetetracarboxylic dianhydride (pyromellitic dianhydride = PMDA) and 4,4′-diaminodiphenyl oxide (4,4′-oxydianiline = ODA) in *N*,*N*′-dimethylacetamide (DMAc). ODA (97%), PMDA (97%), and anhydrous DMAc, stored under argon, were used as purchased (Aldrich Chemical Co.). ODA was dissolved in anhydrous DMAc at room temperature under argon atmosphere. A stoichiometric amount of PMDA in DMAc was then added, and the solution obtained was kept at room temperature while stirring under argon atmosphere. A viscous yellow solution was obtained consisting of the precursor polyamic acid in DMAc.

Polyimide films were prepared by casting the polyamic acid solution onto a glass plate by the tape-casting technique and heating the film 300 °C under vacuum. After cooling to room temperature, the films were easily removed by soaking them in hot distilled water and pealing them off the plate. Typical thickness was 15−20 μm.

For the preparation of polyimide−silica composites, tetramethoxysilane (TMOS) (used as received, ABCR) and deionized water (18 MΩ) were added to the polyamic acid solution, and a homogeneous solution was obtained after stirring at room temperature. Polyimide−silica composite films were then prepared using the same procedure as for the pure polyimide films. A typical thickness obtained was ∼25−30 μm.

The hydrolysis ratio (defined as the molar ratio $h = H_2O/TMOS$) was equal to the stoichiometric amount of water needed to hydrolyze one TMOS molecule ($h = 4$). For silica content variation, different proportions of TMOS were added into the polyamic acid solution.

The samples were denoted by "*x*" where *x* represents the TMOS molar fraction × 100. Table 1 summarizes the compositions obtained for different starting mixtures of the polyamic acid and TMOS.

2. Materials Characterization. Samples containing various amounts of TMOS have been structurally characterized, and the results were compared as a function of the TMOS proportion. Scanning electron micrographs were obtained by HITACHI S-4500 microscope. All samples were platinum coated (2−3 nm) and mounted on aluminum mounts with silver cement. Energy-dispersive X-ray analysis (EDX) was performed on 1 μm thickness with a LEICA Stereoscan 260 system. Density measurements have been made using liquid picnometry at 20 °C in toluene. Thermogravimetric analysis was performed on a Setaram TG 85 apparatus using a 10 °C/min heating rate in air.

A dynamic mechanical thermal analysis apparatus (DMTA MkIII Rheometrics Scientific) was used to measure the viscoelastic response of the polymer films. The samples were kept at 150 °C for 5 min prior to a temperature scan at 3 °C/min from 150 to 450 °C at frequency of 3 Hz. The temperature of the maximum in the tan δ curves was defined as the glass transition temperature (T_g).

X-ray diffraction measurements have been performed with a Bruker diffractometer D-5000 (Cu Kα radiation, $\lambda = 0.154$ nm). The films were taped on monocrystalline (004) silicon wafers to reduce background scattering. The $\lambda/2$ contamination (002) peak was removed from the final diffractograms where necessary.

Small-angle X-ray scattering (SAXS) experiments have been performed using two instruments, both having an incident wavelength equal to 0.154 nm (λ Cu Kα1). One is a low-resolution instrument where the data are collected using a position sensitive detector and a slit collimation system. These experimental parameters allow studies in a range of wave vectors q from 0.2 to 2 nm^{-1}. The scattering curves have been corrected for a scattering background and were desmeared using two methods: an iterative method[17] and another method proposed by Strobl[18] which determines the inverse of the apparatus function. Both procedures gave the same result.

The second instrument uses a high-resolution Bonse−Hart camera. The monochromator is a three-reflection channel-cut germanium crystal and an another channel cut to analyze the scattered beam. These experimental parameters allows studies in a range of wave vectors q from 0.02 to 1 nm^{-1}. Thus, there is an overlap in the range of wave vectors of the two instruments between 0.2 and 1 nm^{-1}.

3. Gas Transport Measurements. The gas permeation properties of the films were determined from measurements of pure gas fluxes. A preliminary high vacuum (10^{-3} Pa) desorption was performed for 48 h at 50 °C and 4 h at 150 °C. Above 72% TMOS, films were brittle and unusable for permeation experiments. Thus, permeation experiments have been performed on samples 0, 25, 60, and 72.

Experiments were done by measuring flows through the membrane at a constant pressure drop over the sample ΔP equal to 1×10^5 Pa. The pressure increase at the downstream side volume (29.9 cm^3) was recorded by a MKS Baratron pressure sensor with a range of 0−1 kPa. Measurements were taken between 50 °C and 150 °C. The gas permeation area was 16.6 cm^2. The permeability curves had a transient and a steady-state portion except for helium. A permeability coefficient (P) was calculated from the slope and a diffusion coefficient (D) was calculated from the extrapolation of the linear steady-state portion to the time axis, the so-called time lag τ:

$$D = l^2/6\tau$$

where l is the membrane thickness.

Gases (purity of 99.9%) having various kinetic diameters (given in parentheses) were used for this study:[19] helium (2.6 Å), oxygen (2.92 Å), carbon dioxide (3.23 Å), nitrogen (3.64 Å), and methane (3.8 Å).

(17) Lake, J. A. *Acta Crystallogr.* **1967**, *23*, 191.
(18) Strobl, G. R. *Acta Crystallogr.* **1970**, *A26*, 367.
(19) Kumins, C. A.; Kwei, T. K. *Diffusion in Polymers*; Crank, J., Park, G. S., Eds.; Academic Press: London, 1968, 107.

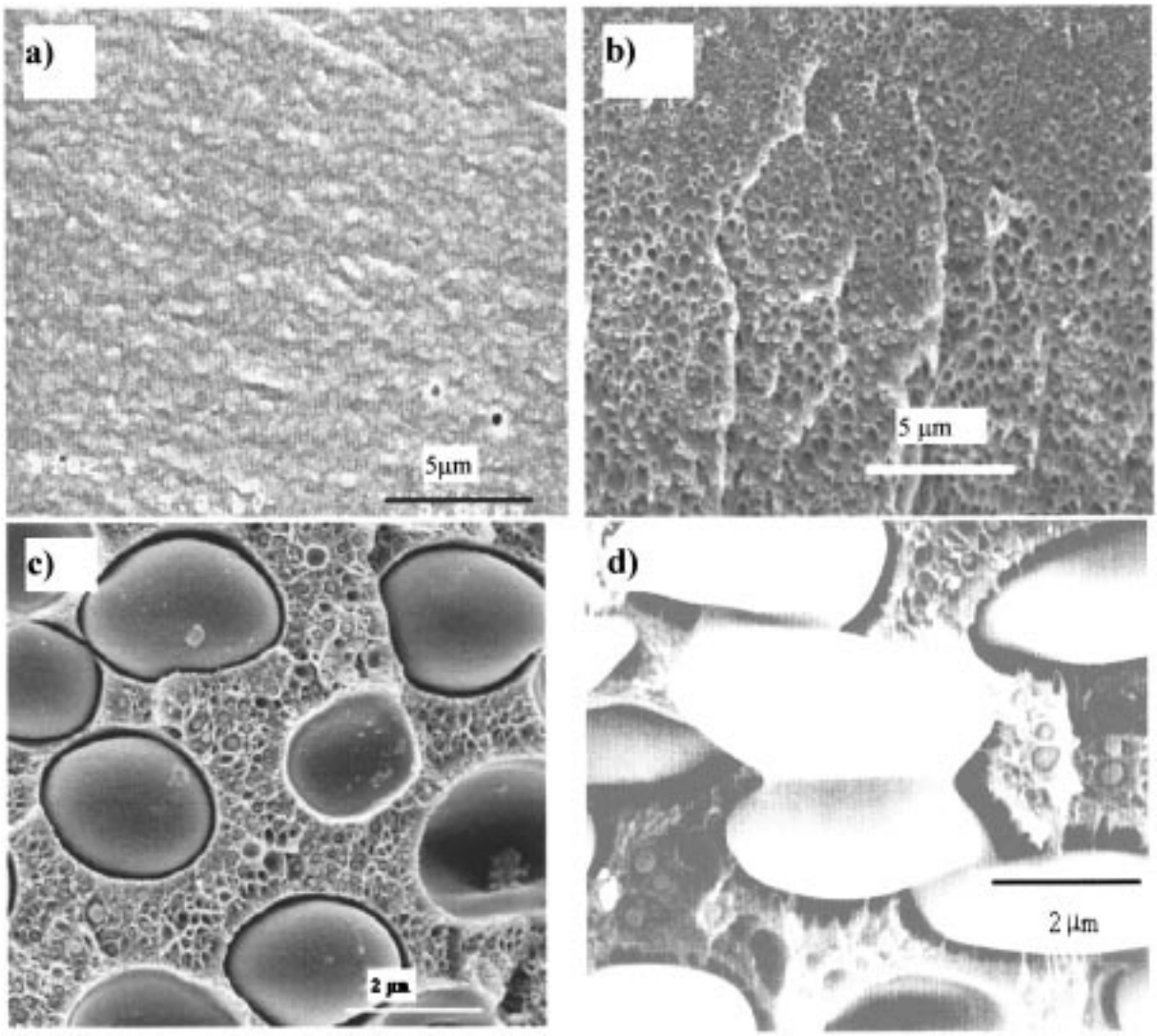

Figure 1. SEM micrographs: sample 25 (a) presents an homogeneous microstructure in the cross section of the film, sample 60 (b) and 72 (c) present a biphasic microstructure in the cross section of the film with silica particles embedded in a polymer matrix. For sample 72, the distribution of the silica particles size is bimodal. Sample 83 (d) shows silica particles coalescence phenomenon.

4. Sorption measurements. CO_2 solubility in polymers has been studied using the pressure decay method[20] at various temperatures between 30 and 150 °C and 10^5 Pa using the manifold of a Micromeretics ASAP 2000 apparatus. The gas concentration relative to the membrane volume is expressed in units of $meter^3_{STP}/meter^3$. To determine the feasibility of such experiments, some gravimetric measurements have been performed with a Setaram TGA92 microbalance.

The analysis of the isotherms has been performed using the dual sorption model in polymer matrixes.[21] This model makes the assumption that the penetrant gas molecules dissolved in the polymer are distributed in two distinct populations. First, there is a Henry-type dissolution (randomly mixed with weak interactions) where the concentration C_d of the gas in the sample increases behaves linearly with the gas pressure. Second, there is a Langmuir-type sorption where the concentration C_h depends on the pressure due to two different factors: the affinity constant b and the maximum sorption capacity of the polymer C'_H. The overall penetrant constant C corresponds to the addition of these two contributions:

$$C - C_d + C_h = k_D P + C'_H bP/(1 + bP) \quad (1)$$

Results

1. Material Characterization. *Macroscopic Evaluation of the Microstructure.* Micrographs of the films showed that samples 0 and 25 were homogeneous (Figure 1a) while samples 60, 72, and 83 were made of silica particles embedded in a polyimide matrix (Figure 1b). Moreover, there were two populations of silica particles (Figure 1c): a population made of small particles of 50−150 nm average diameter and a second population of particles several micrometers in dimension. A coalescence phenomenon is observed for sample 83 between the biggest silica particles (Figure 1d). As previously observed,[2,5,12,15] depending on the composition of the sample, the diameter of the larger particles varied from 1 μm (sample 60) to 7 μm (sample 83). We also showed in previous studies that the silica particle size depends on the hydrolysis ratio.[15]

In samples 60, 72, and 83, EDX analysis (Figure 2) defined the composition of the two components: the matrix was made of carbon, nitrogen, and oxygen and the particles in samples 60, 72, and 83 were made of silicon and oxygen in a ratio O/Si = 2. In sample 25, EDX analysis showed the presence of silicon elements.

(20) Koros, W. J.; Paul, D. R. *J. Polym. Sci. Polym. Phys.* **1976**, *14*, 1903.
(21) Michaels, A. S.; Vieth, W. R.; Barrie, J. A. *J. Appl. Phys.* **1963**, *34*, 1.

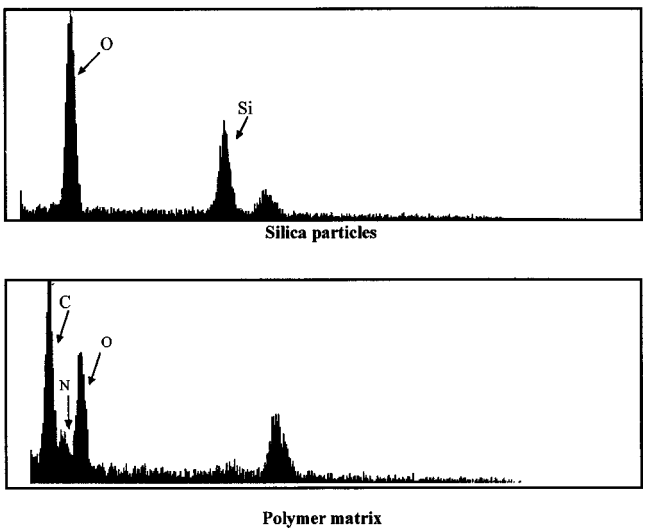

Figure 2. EDX results for polymer matrix (a) and silica particles (b).

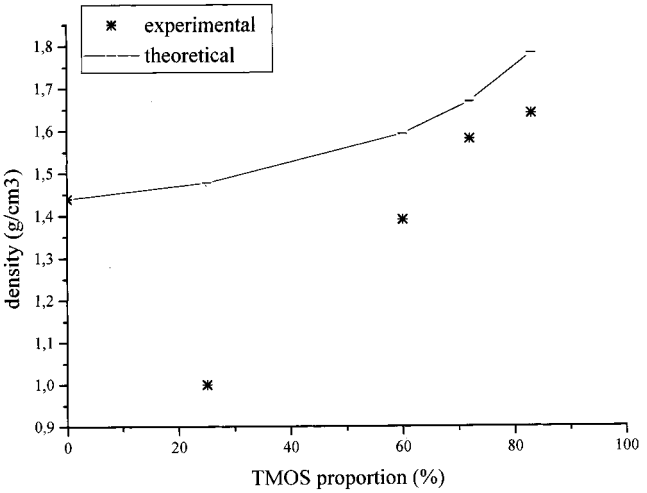

Figure 3. Density variation of the polyimide−silica films as a function of the TMOS proportion. Experimental and theoretical variation are plotted for comparison.

The experimental silica content in the composite films was determined by thermogravimetric measurements from the weight of the final residue after a 750 °C heat treatment in air. The silica content obtained after the TGA experiments (Table 1) was always ~5% lower than the theoretical proportion except for sample 72. This fact has also been reported for other compositions.[15]

The addition of silicon species to the polyimide induces a variation in density (Figure 3). For sample 25, a decrease in density of 30% is observed compared to pure polyimide. Then, the density increases with the TMOS concentration.

Relaxation. Five compositions (0, 25, 60, 72, and 83) have been compared to the pure polyimide film. The glass transition temperatures have been compared as a function of the sample composition (Table 2). A large increase in the glass transition temperature (+13 °C) is observed for sample 25.

When the proportion of TMOS in the polymer is above 60%, the glass transition temperature begins to decrease rapidly. More silica in the film broadens the peaks.

Structural Analysis. The eventual presence of crystalline domains within the polyimide−silica films was checked with wide-angle X-ray diffraction (WAXD). Diffractograms of composite polyimide−silica films were recorded and compared with that of amorphous silica and that of pure polyimide. All patterns of the composite materials showed two diffraction peaks (Figure 4), the first at $2\theta \sim 5°$ being rather small, whereas the second at $2\theta \sim 19-21°$ being broader. Pure polyimide showed a profile with a large peak centered at $2\theta \sim 19.6°$; the corresponding peak of samples 25 and 60 was slightly shifted toward a larger d spacing ($2\theta \sim 19°$) and that of samples 72 and 83 toward a smaller d spacing ($2\theta \sim 21°$). The presence of silica in the material induced a broadening of the large peak. The small peak at high d spacings showed less systematics, but appears to be related with the pure polyimide. It is noted that the diffuse peak of amorphous silica is centered at $2\theta \sim 24°$.

SAXS experiments have been performed to obtain information on the structural feature in these composites. SAXS intensity profiles obtained for sample 25 did not show any interference patterns and the recorded curves were flat while profiles recorded for composite samples all showed all the same evolution between 0.02 and 2 nm^{-1} (Figure 5).

2. Gas Transport. Permeation experiments have been done at 50 °C on samples prepared with various proportions of TMOS. All curves showed the same shape (Figure 6). Permeability coefficients and diffusion coefficients have been calculated (Tables 3 and 4). Permeability coefficients were similar for the pure polyimide

Table 2. Glass Transition Temperatures (°C) Obtained from DMTA Experiments[a]

sample	0	25	60	72	83
T_g (°C ± 1 °C)	396	409	411	404	399

[a] The temperature of the maximum in the tan δ curves is defined as the glass transition temperature (T_g).

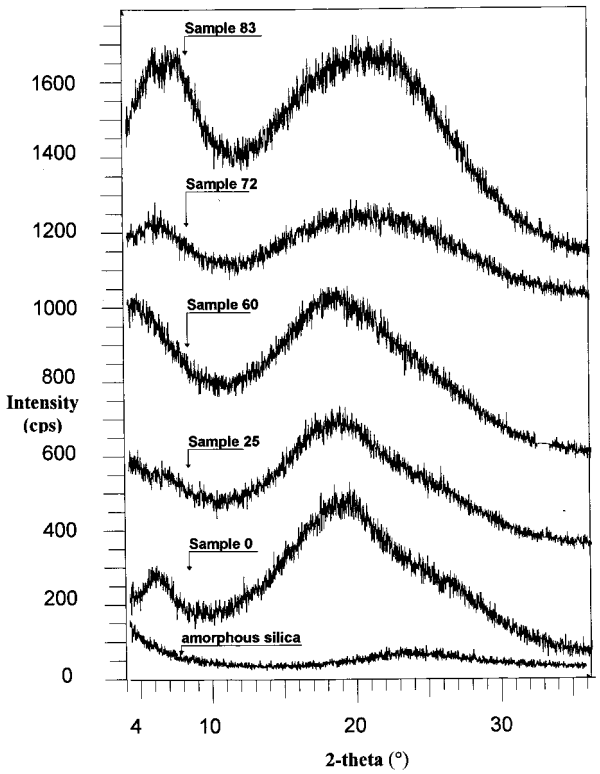

Figure 4. WAXD patterns obtained for various samples.

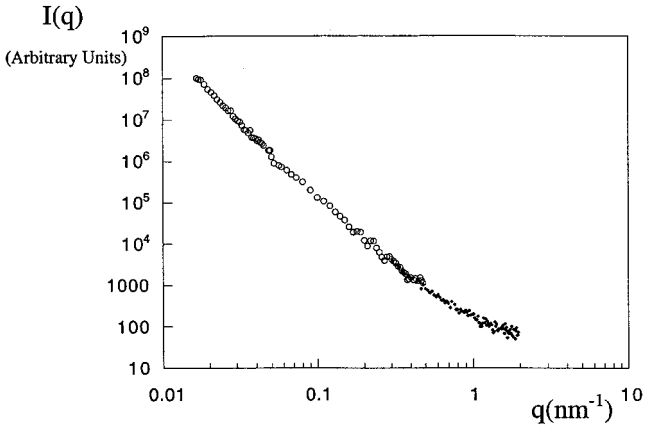

Figure 5. SAXS profile obtained for sample 60.

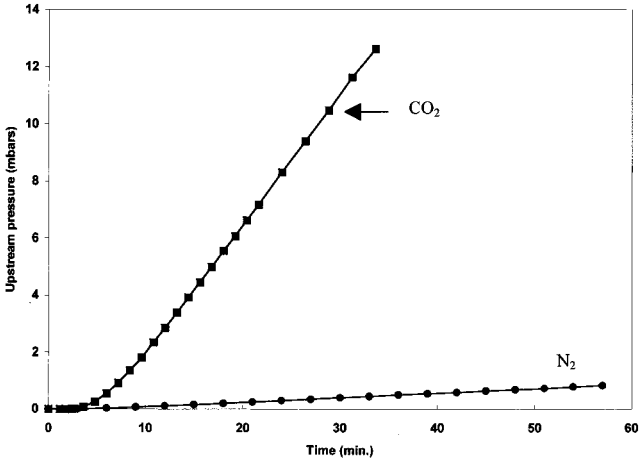

Figure 6. Gas permeation curves obtained at 50 °C for CO_2 and N_2 using sample 60.

Table 3. Gas Permeability Coefficients (Barrer = 10^{-10} cm^3_{STP}, cm/cm^2 s cmHg) (± 3%) at 50 °C Calculated for Various Gases (He, CO_2, O_2, N_2, and CH_4) and Various Sample Compositions

sample	0	25	60	72
P(He)	2.60	2.70	3.40	4.80
P(CO_2)	0.80	1.20	1.50	2.03
P(O_2)	0.17	0.22	0.28	0.38
P(N_2)	0.04	0.04	0.05	0.10
P(CH_4)	0.02	0.03	0.05	0.08

Table 4. Diffusion Coefficients ($10^{-10}$$cm^2$/s) (± 5%) Calculated for Various Gases: CO_2, N_2, and CH_4 (50 °C)

sample	0	25	60	72
D(CO_2)	23	24	34	27
D(N_2)	30	23	44	60
D(CH_4)	5	5.3	7.5	7.9

and sample 25 for He and N_2 and only slightly increased for the other gases (1.4 times). As usual, the fluxes decreased with the kinetic diameter of the gas except for CO_2 because of its high solubility. For samples containing silica particles, regardless of the gas, permeability coefficients increased with the silica proportion by about a factor 2 compared to pure polyimide. For sample 72, if sample 25 is taken as reference, permeability coefficient variation was important (2.4 times) for the two larger gases (N_2 and CH_4) and smaller (1.7 times) for the smaller gases (H_2, CO_2 and O_2).

Concerning the diffusion coefficients (Table 4), their absolute values were not significant because of the

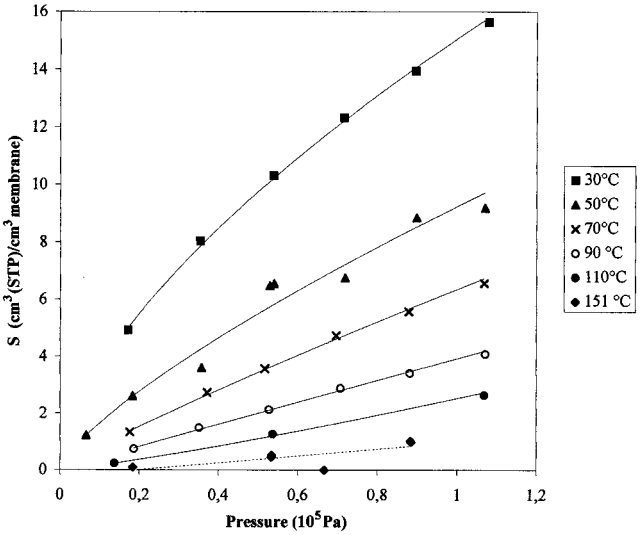

Figure 7. Sorption curves obtained on sample 60 at 50 °C for CO_2.

Table 5. Permeability Activation Energy (kJ/mol) (±1%) for Various Gases and Compositions

sample	He	CO_2	O_2	N_2	CH_4
0	14	13	20	24	29
25	15	10	15	24	24
60	15	9	17	23	22
72	15	10	15	22	15

supposed increased diffusion path length (tortuous paths) produced by the overlapping silica particles. Thus, they will be only compared as a function of the samples composition. No large variation was observed with the silica proportion for CO_2 and CH_4 while N_2 diffusion increased rapidly for samples 60 and 72.

Permeation experiments have been performed for temperatures varying from 50 to 150 °C. Permeability coefficients varied by 2 orders of magnitude in this range of temperatures for CH_4, N_2, and He experiments. Activation energies have been calculated from these data (Table 5). Differences in activation energies between the gases are more important for analysis. Helium, carbon dioxide, and oxygen had lower activation energy (∼10−15 kJ/mol) except for O_2 transport in sample 0, while nitrogen and methane had higher values on the average (∼24 kJ/mol). He and N_2 activation energies did not vary regardless of the composition of the samples while the values of CH_4 activation energies decreased significantly when the silica content increased. For CO_2 and O_2 there was a decreasing step from the pure polyimide to composite samples.

Permeability activation energies decreased when the silica proportion increased. Between 50 and 150 °C, depending on the gas combination, the presence of silica increased the selectivity (He/CO_2, CO_2/O_2), slowed the selectivity decrease (He, CO_2/CH_4), or had no influence (He/N_2). These variations were continuous with the silica proportion. Thus, in contrast to what is generally observed, the increase in permeability due to temperature and the influence of silica enable for certain gas pairs to slightly increase selectivities.

3. Sorption experiments. *a. Sorption coefficients.* Figure 7 shows CO_2 isotherms obtained for sample 60 at different temperatures. For all gases studied, the

Table 6. Sorption Enthalpy (kJ/mol) (±5%) for Various Gases and Compositions

sample	CO_2	N_2	CH_4
0	−22	−7	−14
25	−18	−12	−11
60	−25	−8	−15
72	−23	−6	−13

sorption of the composite film was more pronounced than that of the polyimide.

Variations of solubility with temperature can be written as follows:

$$S - S_0 \exp(-H_s/RT) \quad (2) \qquad (2)$$

where H_s is the sorption enthalpy.

Sorption enthalpies have been calculated from these results (Table 6). They were almost independent of the sample composition. They were low for nitrogen and high for CO_2. Methane activation energies were intermediate.

b. Dual Sorption Model. By fitting the polyimide and composite isotherms with eq 1, k_D, C'_H, and b parameters were determined (Table 7). The isotherms were almost linear for high temperatures (90, 110, and 150 °C). For lower temperatures (<70 °C), the curves were bent concavely.

The trend appeared to be that the Langmuir contribution decreased as the temperature increased ($C,'_H = b = 0$). The temperature variation of these two parameters is given by a decrease from 30 to 150 °C. This decrease was continuous for b, independent of the sample composition. Concerning C'_H, a maximum was observed at about 50 °C for sample 25 and 60. The other compositions exhibit a continuous decrease.

Discussion

1. Materials Characterization. EDX analysis shows the presence of silica (O/Si = 2) in samples 60, 72, and 83 while silicon is present in sample 25 but the presence of silica is excluded. These differences may be explained by the TMOS reaction kinetics during the synthesis. In previous studies,[15] we showed that regardless of the composition, TMOS hydrolysis is completed in less than 1 h and that the polycondensation reactions are faster when the TMOS concentration increases even if they do not proceed completely. Thus, some non-fully-condensed silicon species, stable under imidization, are present in all samples and their proportion decrease with TMOS concentration. Thus, silicon detected by EDX in sample 25 is attributed to noncondensed oligomers for which the low TMOS concentration in the solution did not enable polycondensation to proceed in order to obtain silica in the final material. However, the presence of silicon in the material demonstrates that TMOS has been hydrolyzed and that it did not evaporate during the synthesis. Unfortunately, these species are not concentrated enough to be characterized by ^{29}Si solid-state NMR and thus the chemical structure of that dispersed product is still unknown. Also, one may ask about possible interactions of silica species with the polymer in samples 60, 72, and 83. ^{29}Si NMR experiments[15] in liquid solutions during the synthesis showed that the chemical shifts observed for the silica oligomers during the synthesis were identical to those obtained during TMOS gels synthesis. Solid-state spectra did not reveal any significant chemical shifts to that of pure TMOS gels. When strong interactions between different species occur, large shifts from these standard position are usually observed.[22] Thus, this shows that pure silica clusters are formed in samples 60, 72, and 83.

The difference between the theoretical and experimental proportion of silica (except for one sample) may arise from two facts. First experimental error (±2%) has to be taken into account. Second, the presence in the films of noncondensed silicon oligomers, which are removed by the high-temperature thermogravimetric heat treatment, can contribute to the silicon loss.

Experimental density variation has been compared to theoretical density values calculated assuming ideal mixing of amorphous silica (2.2 g/cm^3) and polyimide (1.4 g/cm^3). This comparison shows that the highest discrepancy between experimental and theoretical values is observed between sample 0 and 60. However ideal mixing is not a good model for this system since the two components densities are not independent with composition. At least, the polyimide does not keep its density as the composition of the material is varied.

Measurements of dynamic mechanical losses provide information on transitions occurring in polymers. Typical values of the loss tangent document the effect of filler on the glass transition temperature. Increase in glass transition temperature of polyimide−silica materials compared to pure polyimide has also been previously observed.[23] It can be interpreted in terms of a reduction of the chain mobility by the silica particles. This can be either due to a physical reticulation between the chains or to weak interactions between the organic and inorganic components. The rheological modification observed by DMTA experiments occurs in two steps. The first step occurs when TMOS is incorporated in the polyimide up to 60%. This induces a variation of 14 °C in the glass transition temperature between the polyimide and samples 25 and 60 which have an average T_g equal to 411.5 ± 2.5 °C. The second step is characterized by a 10 °C gap of the glass transition temperature between the previous two samples and samples 72 and 83 (average T_g = 401.5 ± 2.5 °C). This two-step behavior has been previously observed for similar materials but not interpreted.[3] In the present study, this can be correlated with the density variation with a transition behavior for approximately 60% TMOS proportion. As the chain mobility decreases (higher T_g), the material density decreases and vice-versa. Such combined effects between T_g and density have already been noticed for polymer-like epoxy cross-linking.[24,25] The broadening of the DMTA peaks, moreover, shows that the presence of silicon species in the material involves an heterogeneity in the relaxation times distribution of the polymer chains which increases with the silica proportion. This indicates that the chain length distribution between physical cross-linking points increases with the silica proportion in the sample showing the high heterogeneity

(22) (a) Marsmann, H. *^{29}Si NMR Spectroscopy*; Diehl, P., Ed.; 1981; Vol. 17. (b) Engelhardt, G.; Radeglia, R. *Chem. Phys. Lett.* **1984**, *108*, 271. (c) Smith, J. V.; Blackwell, C. S. *Nature* **1983**, *303*, 223.

(23) Mascia, L.; Kioul, A. *Polym. J.* **1995**, *36*, 3649.

(24) Ennes, J.; Gillham, J. *J. Appl. Polym. Sci.* **1983**, *28*, 2831.

(25) Min, B. G.; Shin, D. K.; Stachurski, Z. H.; Hodgkin, J. H. *Polym. Bull.* **1994**, *33*, 465.

Table 7. CO_2 Sorption Parameters Analyzed with the Dual Sorption Theory for Various Compositions

sample		0	25	60	72	83
30 °C	C'_H	12.7	4.8	10.3	11.3	23.2
	k_D	7.7×10^{-3}	9.5×10^{-3}	9.3×10^{-3}	12.5×10^{-3}	10.4×10^{-3}
	b	3.3×10^{-3}	6.8×10^{-3}	4.3×10^{-3}	4.4×10^{-3}	2.5×10^{-3}
50 °C	C'_H	8	14.9	16.4	9.9	15.5
	k_D	6.3×10^{-3}	4.9×10^{-3}	1.8×10^{-3}	8.1×10^{-3}	10.1×10^{-3}
	b	2.4×10^{-3}	6.1×10^{-4}	1.1×10^{-3}	2.2×10^{-3}	1.4×10^{-3}
70 °C	C'_H	2.8	0	4.4	−	−
	k_D	6.6×10^{-3}	7.5×10^{-3}	5.5×10^{-3}	−	−
	b	1.8×10^{-3}	0	1.3 × 10−3	−	−
90 °C	k_D	5.3×10^{-3}	5×10^{-3}	5.0×10^{-3}	7.1×10^{-3}	9×10^{-3}
110 °C	k_D	3.7×10^{-3}	3.3×10^{-3}	3.2×10^{-3}	4.2×10^{-3}	5.9×10^{-3}
150 °C	k_D	2.1×10^{-3}	2.5×10^{-3}	1.4×10^{-3}	2.6×10^{-3}	3.2×10^{-3}

of the physical composite network. Thus, the polymer is physically cross-linked with a large distribution in molecular weight between cross-linking points.

The WAXD experiments give a hint on the origin of this two-step behavior. Since the spectra do not reveal small and well-defined peaks, the materials have to be amorphous. The diffraction peak at low angles is related to intramolecular order at shorter length scales, whereas the diffuse peak around $2\theta \sim 19-21°$ originates from coherent scattering between the molecular chains at even shorter length scales.[26] The intensity ratio of the low angle peak to the high angle peak has the tendency to increase with increasing TMOS proportion. This might indicate that the chain structure in the composite material is slightly modified by the introduction of silicon species in the polyimide. The reduction in d spacing for samples 72 and 83 could be the result of steric effects, chains getting closer when silica particles increase in size. The reduction could however equally well be apparent, since the introduction of TMOS gives rise to more scattering from this component. This might broaden and shift the peak toward the central maximum of silica at $2\theta \sim 24°$.

At a scale between 0.02 and 2 nm^{-1}, the comparison between the SAXS profiles of all composites with the polyimide reference showed that the effect of silicon species is marked at small scattering vectors ($q < 1$ nm^{-1}). SAXS spectra of sample 25 reveal no diffuse scattering at small wave vectors. As sample 25 does contain silicon (detected by EDX), this is more proof for a homogeneous polymer distribution without silica segregation. On the other hand, all samples containing silica particles present the same SAXS profile. As there are no pores in these materials, the contribution of the microstructure to the scattering is only due to the silica particles. Thus, the similarity of the SAXS profiles indicates a similarity between the materials structural features in this range of scattering vectors (i.e., 0.5−50 nm) which is independent with the TMOS concentration. The Guinier region (at small wave vectors) is not yet observed in this wave vectors range, indicating that the size of the aggregates is greater than 50 nm.

2. Gas Transport Properties. Gas transport within microporous membranes (pore diameter <2 nm) is generally described as microporous diffusion following Lennard-Jones potential criteria.[27] Meanwhile, gas transport through nonporous membranes is described as a dissolution−diffusion process.[28] This mechanism can be described in three steps: (1) dissolution or adsorption of the gas at the "entry" interface; (2) molecular diffusion inside the solid which is in general the slower step; and (3) desorption of the gas at the "exit" interface.

With regard to the gas transport, it is well-known that if the silica particles were dense and the polymer matrix identical to its polyimide reference, a decrease in the gas permeability should be observed with the addition of silica. As this is not the case here, there are two possible mechanisms: the gas transport can occur through the particles (if the silica particles are porous) or in the interfacial region between the particles and the matrix. As the gas permeability increases with an increase of silica proportion, the hypothesis of porous silica particles is valuable. Nevertheless, the gas permeability coefficients measured for high silica proportion are not similar to the values reported for microporous silica.[27] Thus, the contribution of the interfacial region to the gas transport mechanism may be possible. Indeed, silica particles introduction may affect the morphology of the matrix by creation of a particle−matrix interphase and thus influence the gas transport. The overall permeability would then be a function of the matrix permeability and the interface permeability.

Diffusion coefficients D that have been calculated are effective values which include Henry and Langmuir contributions. Due to the experimental averaging over a pressure range from 0 to 0.1 MPa, to calculate D for each contribution, it would be necessary to measure the permeability as a function of pressure. Moreover, this would enable to compute the Langmuir/Henry ratio and thus measure the selectivity and productivity of the Langmuir contribution compared to simple sorption.

Conclusion

Polyimide−silica composite materials have been prepared via the sol−gel process with various TMOS proportion. The influence of the silica proportion on the gas transport properties has been evaluated.

The structural characteristics of the materials have been studied. Micrographs showed that samples prepared with 25% TMOS are homogeneous while above, the microstructure is made of silica particles embedded in a polyimide matrix. The homogeneity of low TMOS concentration materials has been attributed to noncondensed species present in the material. These species result in a significant decrease in density but above 50% TMOS, increasing TMOS concentration contributes to

(26) Han, H.; Gryte, C. C.; Ree, M. *Polym. J.* **1995**, *36*, 1663.
(27) Delange, R. S. A.; Keizer, K.; Burgraaf, A. J. *J. Membr. Sci.* **1995**, *104*, 81.
(28) Graham T. *Philos. Mag.* **1866**, *32*, 401.

a higher density. SAXS experiments confirmed the homogeneity of the networks built with 25% TMOS. Above 25% TMOS, this technique showed that the structure of the silica aggregates is independent of the silica concentration.

X-ray diffraction experiments shows that the chain structure in the material is modified by the presence of silicon species. These modifications were also observed by the variation of glass transition temperature which first increases and decreases rapidly when the proportion of TMOS is above 60%. Moreover, the damping peak of tan δ becomes broader with increasing silica contribution.

Gas permeation experiments with He, O_2, N_2, CO_2, and CH_4 have been carried out on the polyimide−silica materials. The presence of silicon species increases the permeability coefficients without, for some gas pairs, the usual loss in selectivity in the 50−150 °C temperature range.

CO_2 sorption experiments have been analyzed using the dual sorption mode theory. Langmuir and Henry contributions have been evaluated. At high temperature, the Henry contribution is predominant.

Although density, T_g, or d spacing experiments have been done as indirect measurements of free volume, correlations of the gas transport properties with the structural properties are not strongly identified. Experiments that measure permeation as a function of pressure for various temperatures would be needed to gain a better understanding of the transport mechanism. This will be the focus of a future study.

Acknowledgment. We thank Georges Nabias and Didier Cot for their contributions to SEM microscopy, Marcel Lopez for the thermogravimetric analysis, Arie Van der Lee for X-ray diffraction experiments and Patrice David for his contribution to computer calculations. We also thank S. Guilbert (Inra, Montpellier) for DMTA experiments. C.J. and M.S. acknowledge the financial support provided by the European Commission through a Joule Program JOU2-CT92-0084. M.S. and R.D.N. acknowledge the financial support from NATO through grant CRG 970370. The authors also thank an anonymous reviewer for constructive comments.

CM9805018